Title

Healthy brain connectivity predicts atrophy progression in non-fluent variant of primary progressive aphasia

Journal

Brain, 139(10)

ISSN

0006-8950

Authors

Mandelli, Maria Luisa
Vilaplana, Eduard
Brown, Jesse A
et al.

Publication Date

2016-10-01

DOI

10.1093/brain/aww195

Peer reviewed

doi:10.1093/brain/aww195 BRAIN 2016: 139; 2778–2791 | 2778

BRAIN
A JOURNAL OF NEUROLOGY

Healthy brain connectivity predicts atrophy progression in non-fluent variant of primary progressive aphasia

Maria Luisa Mandelli,[1] Eduard Vilaplana,[2,3] Jesse A. Brown,[1] H. Isabel Hubbard,[1] Richard J. Binney,[4] Suneth Attygalle,[1] Miguel A. Santos-Santos,[1] Zachary A. Miller,[1] Mikhail Pakvasa,[1] Maya L. Henry,[5] Howard J. Rosen,[1] Roland G. Henry,[6,7,8] Gil D. Rabinovici,[1] Bruce L. Miller,[1] William W. Seeley[1,9] and Maria Luisa Gorno-Tempini[1]

Neurodegeneration has been hypothesized to follow predetermined large-scale networks through the trans-synaptic spread of toxic proteins from a syndrome-specific epicentre. To date, no longitudinal neuroimaging study has tested this hypothesis *in vivo* in frontotemporal dementia spectrum disorders. The aim of this study was to demonstrate that longitudinal progression of atrophy in non-fluent/agrammatic variant primary progressive aphasia spreads over time from a syndrome-specific epicentre to additional regions, based on their connectivity to the epicentre in healthy control subjects. The syndrome-specific epicentre of the non-fluent/agrammatic variant of primary progressive aphasia was derived in a group of 10 mildly affected patients (clinical dementia rating equal to 0) using voxel-based morphometry. From this region, the inferior frontal gyrus (pars opercularis), we derived functional and structural connectivity maps in healthy controls ($n = 30$) using functional magnetic resonance imaging at rest and diffusion-weighted imaging tractography. Graph theory analysis was applied to derive functional network features. Atrophy progression was calculated using voxel-based morphometry longitudinal analysis on 34 non-fluent/agrammatic patients. Correlation analyses were performed to compare volume changes in patients with connectivity measures of the healthy functional and structural speech/language network. The default mode network was used as a control network. From the epicentre, the healthy functional connectivity network included the left supplementary motor area and the prefrontal, inferior parietal and temporal regions, which were connected through the aslant, superior longitudinal and arcuate fasciculi. Longitudinal grey and white matter changes were found in the left language-related regions and in the right inferior frontal gyrus. Functional connectivity strength in the healthy speech/language network, but not in the default network, correlated with longitudinal grey matter changes in the non-fluent/agrammatic variant of primary progressive aphasia. Graph theoretical analysis of the speech/language network showed that regions with shorter functional paths to the epicentre exhibited greater longitudinal atrophy. The network contained three modules, including a left inferior frontal gyrus/supplementary motor area, which was most strongly connected with the epicentre. The aslant tract was the white matter pathway connecting these two regions and showed the most significant correlation between fractional anisotropy and white matter longitudinal atrophy changes. This study showed that the pattern of longitudinal atrophy progression in the non-fluent/agrammatic variant of primary progressive aphasia relates to the strength of connectivity in pre-determined functional and structural large-scale speech production networks. These findings support the hypothesis that the spread of neurodegeneration occurs by following specific anatomical and functional neuronal network architectures.

1 Department of Neurology, Memory and Aging Center, University of California San Francisco, CA, USA
2 Memory Unit, Department of Neurology, Hospital de la Santa Creu i Sant Pau - Biomedical Research Institute Sant Pau – Universitat Autonoma de Barcelona, Spain
3 Centro de Investigacion Biomedica en Red de Enfermedades Neurodegenerativas – CIBERNED, Spain
4 Department of Communication Sciences and Disorders, Temple University, Philadelphia, Pennsylvania, USA

Received February 12, 2016. Revised May 16, 2016. Accepted June 2, 2016. Advance Access publication August 6, 2016

5 Department of Communication Sciences and Disorders, University of Texas, Austin, USA
6 Department of Neurology, University of California San Francisco, CA, USA
7 Bioengineering Graduate Group, University of California Berkeley, San Francisco, CA, USA
8 Department of Radiology and Biomedical Imaging, University of California San Francisco, San Francisco, CA, USA
9 Department of Pathology, University of California San Francisco, CA, USA

Correspondence to: Maria Luisa Mandelli,
675 Nelson Rising Lane, Mission Bay Campus,
San Francisco, CA 94158,
USA
E-mail: MariaLuisa.Mandelli@ucsf.edu

Keywords: functional connectivity; tractography; longitudinal atrophy; primary progressive aphasia; connectivity

Abbreviations: FTLD = frontotemporal lobar degeneration; IFGop = inferior frontal gyrus pars opercularis; nfvPPA = non-fluent/agrammatic variant of primary progressive aphasia; SMA = supplementary motor area

Introduction

Syndrome-specific patterns of atrophy in various neurodegenerative diseases mirror healthy structural and functional network architecture, perhaps due to trans-synaptic spread of abnormally folded proteins through connected neuronal pathways (Clavaguera *et al.*, 2009; Frost and Diamond, 2010; de Calignon *et al.*, 2012; Liu *et al.*, 2012). Within this framework, at early disease stages, pathological changes occur in a specific region of the brain (epicentre) that is especially vulnerable to each disorder (Zhou *et al.*, 2012). From there, the disease spreads over time along pathways that are most connected to the epicentre, reaching other regions by following the architecture of predetermined large-scale neuronal networks, as defined in healthy control subjects. Through this process, each syndrome results in network-specific patterns of neuroimaging changes that can be detected by cross-sectional structural and functional neuroimaging studies (Seeley *et al.*, 2009; Raj *et al.*, 2012). An example of network-specific neurodegeneration is the non-fluent/agrammatic variant of primary progressive aphasia (nfvPPA), a neurodegenerative syndrome most commonly caused by frontotemporal lobar degeneration (FTLD)-tau pathology (Josephs *et al.*, 2006; Mesulam *et al.*, 2008; Grossman, 2011; Caso *et al.*, 2014; Santos-Santos *et al.*, 2016) and consistently associated with specific neuroimaging changes in the speech production network. This circuit includes the left inferior frontal, dorsal insular, supplementary motor and striatal grey matter regions (Grossman *et al.*, 1996; Nestor *et al.*, 2003; Gorno-Tempini *et al.*, 2006) and connecting white matter pathways (Galantucci *et al.*, 2011; Catani *et al.*, 2013; Mandelli *et al.*, 2014). Damage to this network results in the motor speech and grammatical deficits typical of nfvPPA. The natural history of the disorder often evolves into a more general motor syndrome such as progressive supranuclear palsy or corticobasal degeneration syndromes.

Cross-sectional neuroimaging studies relating patterns of atrophy to functional connectivity in healthy subjects have found that nfvPPA and other neurodegenerative diseases target specific networks (Seeley *et al.*, 2009). Longitudinal neuroimaging experiments are necessary, however, to demonstrate that the pattern of disease progression through the networks is related to the strength of connectivity between the epicentre and later-affected regions in the healthy brain. NfvPPA is a particularly good model to study the relationship between longitudinal atrophy and connectivity strength in controls for several reasons: (i) it is usually diagnosed at an early stage, thus allowing easy identification of the syndrome-specific epicentre; (ii) it involves an anatomically well-known neural network of grey and white matter structures, the speech production network; and (iii) it is most often caused by FTLD-tau pathology, and tau aggregates have been shown to spread trans-synaptically in experimental models.

Here, we used multimodal MRI techniques to investigate the pattern of longitudinal brain atrophy in a large cohort of nfvPPA patients and relate it to healthy functional and structural network architecture. First, we identified the nfvPPA syndrome-specific epicentre in a cohort of patients in the early stage of the disease. Then, we derived the functional and structural connectivity of this region in a group of matched healthy controls. Last, we investigated the relation between structural network architecture, strength of connectivity in healthy controls and longitudinal changes in a large cohort of 34 patients with nfvPPA using correlation and graph theoretical analyses. We hypothesized that the longitudinal progression of atrophy in nfvPPA would selectively follow the functional and structural speech production network anchored by the epicentre in the inferior frontal gyrus. These findings would provide the first *in vivo* confirmation of prion-like, network-specific progression of disease. This has major implications for understanding disease pathogenesis and for tracking efficacy of therapeutic agents.

Materials and methods

Subjects

We identified all patients at the Memory and Aging Center of the University of California, San Francisco (UCSF MAC) who

met the international criteria for diagnosis of nfvPPA. We identified 34 patients with nfvPPA who had undergone a baseline high-resolution T_1-weighted MRI and 1-year follow-up. All subjects underwent detailed neurological, cognitive and neuropsychiatric evaluation. Post-mortem pathological evaluation was available in 23 cases and amyloid PET molecular imaging in 9 of the remaining 11. Of the 23 with pathological confirmation, 91% ($n = 21$) had evidence of FTLD-tau pathology (4Rtau in 19, Pick's disease in two) and 9% ($n = 2$) had TDP-A pathology. Amyloid imaging was negative in all nine cases for which it was available. Of the 11 patients, eight are still being followed at the UCSF MAC. Two of the 11 have developed progressive supranuclear palsy syndrome within 3 years of their first visit. Two developed corticobasal degeneration syndrome within 1 year of their first visit.

Healthy control subjects without cognitive or neurological deficits were selected from the UCSF MAC database. We studied a total of 72 healthy controls with a baseline T_1-weighted MRI and completed 1-year follow-ups to compare typical longitudinal volume changes. An additional 30 healthy controls completed resting-state functional MRI and high angular resolution diffusion-weighted imaging (HARDI), to investigate healthy structural and functional connectivity.

Informed consent was obtained from all participants according to the Declaration of Helsinki and approval was obtained from the UCSF Committee on Human Research.

Cognitive and language evaluation

Patients underwent neuropsychological assessments (Kramer *et al.*, 2003) and speech and language evaluations (Gorno-Tempini *et al.*, 2004; Wilson *et al.*, 2010) at baseline and at follow-up.

Neuropsychological evaluation

The neuropsychological screening battery has been previously described (Rosen *et al.*, 2002; Gorno-Tempini *et al.*, 2004). General intellectual functioning was assessed with the Mini-Mental State Examination (MMSE). Memory tests included the California Verbal Learning Test – Short Form (CVLT-SF) and 10-minute free recall of the Benson complex figure. Copies of the Benson figure and the number location test from the Visual Object Space Perception (VOSP) battery provided a measure of visuospatial functioning. Attention, speed, working memory and executive function tests included phonemic fluency (words beginning with 'D' generated in 1 min), design fluency (Delis-Kaplan Executive Functions System – Trial 1), a modified version of the Trails B test, forward and backward digit span, the Stroop colour naming and interference tasks, the alternating M and N test, and abstract reasoning (similarities and proverbs). Patients were also asked to perform five simple arithmetic calculations. Initial speech and language screening included the abbreviated (15-item) Boston Naming Test (BNT), semantic fluency (animals generated in 1 min), oral repetition, verbal agility (consisting of timed rapid repetition of multi-syllabic words), syntax comprehension (the BDAE cards 60 through 64), vocabulary comprehension (the Peabody Picture Vocabulary Test – Revised, PPVT-R), and regular and irregular word reading.

Speech and language evaluation

In addition to the initial speech and language screening included in the neuropsychological screening battery, patients with nfvPPA received additional speech and language testing. We used a comprehensive speech and language battery that has been previously described (Gorno-Tempini *et al.*, 2004). The language battery included the Western Aphasia Battery (WAB) (Kertesz, 1980) with the following subtests: Spontaneous Speech (Information content and Fluency), Yes/No Comprehension, Auditory Word Recognition Total Score, Sequential Commands Total Score, and Repetition Total Score. Additional measures included the Motor Speech Evaluation (MSE) Apraxia of Speech Rating, the MSE Dysarthria Rating (Mack *et al.*, 1992), and the CYCLE-R syntactic comprehension subtests (Curtiss and Yamada, 1988).

MRI sequences

Subjects underwent MRI on either a 1.5 T (40% of patients, 50% of controls) or 3 T Siemens scanner (60% of patients, 50% of controls) for the acquisition of T_1 images, the parameters of which are previously described (Mandelli *et al.*, 2016). Resting-state functional MRI and HARDI sequences were acquired in an additional group of 30 healthy subjects at the 3 T scanner. Resting-state functional MRI data using a T_2*-weighted echo-planar sequence included 240 volumes with 36 AC/PC-aligned axial slices in interleaved order (slice thickness = 3 mm with 0.6 mm gap; field of view = 230 × 230 mm; matrix = 92 × 92; repetition time = 2000 ms; echo time = 27 ms; flip angle = 80°). The subject was asked to lie still with eyes closed, remain awake and think of nothing. HARDI data using a single-shot spin-echo echo-planar imaging (SE-EPI) sequence including 55 contiguous axial slices were acquired in an interleaved order with in-plane resolution = 2.2 mm^2, slice thickness = 2.2 mm, time to repetition time/echo time = 8000/109 ms, flip angle = 90°, matrix = 100 × 100, 64 non-collinear diffusion sensitization directions at b = 2000 s/mm^2, 1 at b = 0, and an integrated parallel acquisition techniques (iPAT) acceleration factor of 2.

General strategy

The analysis consisted of the following steps.

(I) Identify the syndrome-specific epicentre in nfvPPA. We identified the peak area of disease atrophy in nfvPPA. Designating this region as the syndrome-specific epicentre, we hypothesized that the disease would spread along structural and functional connections to downstream areas. For this reason, we first chose a subgroup of patients with nfvPPA ($n = 10$) at the earliest stage of the disease (i.e. Clinical Dementia Rating = 0). We performed a voxel-based morphometry (VBM) analysis to select the peak with the highest Z-score obtained from statistical comparison with a matched group of healthy subjects.

For VBM analysis, structural image processing and statistical analysis were performed using Statistical Parametric Mapping (SPM) software (Wellcome Trust Center for Neuroimaging, London, UK) running under Matlab

R2013a (MathWorks), as described in our previous studies (Mandelli *et al.*, 2016).

(II) Delineate functional connectivity of the epicentre in healthy individuals: intrinsic connectivity analysis. We used the epicentre (X, Y, Z; identified in Step 1) to create a 4 mm radius seed region of interest to define an intrinsic connectivity network (ICN) in 30 healthy subjects with resting-state functional MRI acquisition.

Next, a sphere of 4 mm radius was created in the precuneus ($x = 2$, $y = -51$, $z = 27$; MNI) to define the default mode network (DMN) in the same group of controls. The DMN is an intrinsic connectivity network linking precuneus/posterior cingulate cortex with medial frontal regions and bilateral inferior parietal regions (Greicius *et al.*, 2004; Damoiseaux *et al.*, 2006) and was used as a control ICN to contrast against the nfvPPA epicentre-anchored network.

Preprocessing of the functional images was carried out using tools available in FSL version 5 (http://fsl.fmrib.ox.ac.uk/fsl/fslwiki/), AFNI (http://afni.nimh.nih.gov/afni/), and Numpy in Python version 2.7.3. After discarding the first eight volumes of each run, functional datasets were slice time corrected, spatially realigned, skull-stripped, co-registered to the structural T_1-weighted image, normalized, and smoothed with a 6 mm full-width at half-maximum Gaussian kernel. Co-registration was performed between each subject's anatomical T_1 skull-stripped scan and each subject's mean functional image. Normalization was done by calculating the transformation parameters between the subject's T_1 anatomical image and the MNI T_1-weighted image template and then applying those parameters to the functional dataset. CSF and white matter nuisance variables were then estimated from the data. To define the CSF and white matter regressors, we eroded the FSL's CSF and white matter tissue prior masks and computed the mean time-series of the resulting regions of interest, respectively. Finally, the functional datasets were band-pass filtered ($0.008\,\text{Hz} < f < 0.15\,\text{Hz}$) and the nuisance variables were regressed out from the data, which included the six motion parameters, CSF and white matter time series as well as the first derivative and quadratic terms, as suggested in Satterthwaite *et al.* (2013). Spectral filtering and nuisance regression was combined into a single step using AFNI tools (Hallquist *et al.*, 2013). All preprocessing steps were performed in each subject's native space.

Seed-based connectivity was performed on the preprocessed data in each subject's native space. The selected seed regions of interest were unwarped from MNI standard space using the previously estimated normalization parameters. For each subject, the average time series from the seed was extracted and used to compute the temporal correlation against all the other voxels in the brain to create an r–Pearson correlation map of each voxel's connectivity strength to the seed region of interest. The r–Pearson correlation maps were transformed into Z-scores using Fisher's r to Z transformation and finally, the individual maps were normalized to MNI space for group analysis.

Group-level healthy connectivity maps were derived by performing one-sample t-tests in SPM with a statistical threshold of $P < 0.001$, family wise error (FWE) corrected.

(III) Delineate structural connectivity of the epicentre in healthy individuals: tractography. The coordinates obtained from the VBM were used to create a sphere of 6-mm radius to delineate the white matter pathways in the same group of controls. This region was used as seed for tractography. A slightly larger region of interest compared to the one used for the functional connectivity was chosen to ensure white matter inclusion. Diffusion imaging data processing and tractography were performed with a q-ball probabilistic residual bootstrap method described in previous works (Berman *et al.*, 2008; Mandelli *et al.*, 2014).

An average healthy fractional anisotropy map was obtained after normalization of each control subject to the FMRIB58 fractional anisotropy template in the MNI space using a linear (FLIRT) and non-linear (FNIRT) registration in FSL. The resulting white matter pathways were defined for each control subject and then registered into the MNI space. An average tract was obtained and used as a template mask of the healthy white matter pathways. Finally, the template mask was subdivided in voxels of $4 \times 4 \times 4$ mm^3 volume sizes for subsequent analyses. This subdivision was created solely to provide spatial information along the tract. Tractography should represent the anatomical, structural pathway through which the toxic proteins would spread.

(IV) Graph theoretical network analysis. In previous graph theoretical work, the strongest predictor of a node's atrophy severity was its shortest functional path to the syndrome-related epicentre (Zhou *et al.*, 2012). Based on this model, nodes with shorter paths to the epicentre in health will be associated with greater atrophy severity in disease and greater longitudinal atrophy, as tested in this study.

The graph theory approach consists of formalizing the system as a mathematical network with nodes and edges. First, we defined the nodes by subdividing the intrinsic connectivity map obtained from the healthy control group into non-overlapping cubes with $8 \times 8 \times 8$ mm^3 grey matter volume, yielding a total of n nodes. This subdivision was created to obtain a manageable number of nodes for the subsequent analyses. The relationships between nodes are defined as the Pearson's correlation coefficient between node pairs. For each subject, the mean time series from each node was correlated with every other node in a pairwise fashion to determine the connectivity matrix. The group connectivity matrix was calculated by averaging individual subject matrices and then performing Fisher's Z transformation.

The node that enveloped the peak atrophy coordinate was identified as the epicentre node. Every other node's connectivity strength to the epicentre was then obtained by extracting the epicentre node's row from the group connectivity matrix. We then calculated the shortest intrinsic functional path of each node to the epicentre (i.e. the sum of the edge weights forming the shortest path from node i to the epicentre node) (Rubinov and Sporns, 2010).

We further applied a modularity approach to divide the inferior frontal gyrus pars opercularis (IFGop) epicentre-seeded network into subnetworks of highly interconnected nodes (subgraphs), such that nodes within subgraphs were more densely connected to one another than to the rest of the graph (Newman, 2006). We used the Louvain method, which divided the network into non-overlapping subsets of nodes (i.e. modules) so that the number of intramodular edges was maximal and the number of intermodular edges was minimal (Blondel *et al.*, 2008).

We used in-house Matlab programs based on the BGL graph library developed by Davis Gleich (https://github.com/dgleich/matlab-bgl). Mathematical notation can be found in Rubinov and Sporns (2010).

(V) Determine longitudinal changes in all nfvPPA patients versus controls. Longitudinal regional brain volume changes were estimated using the Pairwise Longitudinal Registration Toolbox implemented in SPM12b (version 5298) (Ashburner and Ridgway, 2012), which addresses concerns regarding asymmetric bias in pair-wise longitudinal registration (Thomas *et al.*, 2009; Yushkevich *et al.*, 2010). The process first consists of intra-subject registration, using iterative and interleaved rigid-body alignment, as well as diffeomorphic warping and correction for differential intensity inhomogeneity to generate a within-subject template representing an average of the subject's two scans with respect to position, shape and intensity non-uniformity. Two Jacobian determinant maps are computed; one that describes the relative difference in volume between the first scan and the average template, and another between the second scan and the template. These maps are generated in the same image space as the within-subject average. Computing the difference between these two Jacobian determinants provides a map of relative change in volume between scan one and scan two at each spatial location. These maps were divided by the interscan interval (as a proportion of a year) to become maps of annual rate of relative volume change.

To allow statistical analysis in standardized space, each subject's average image was bias corrected and the brain was partitioned into grey matter, white matter, and CSF, using the unified segmentation procedure. Mappings from the grey and white matter segments of the within-subject averages (all patients and control subjects) to an iteratively evolving study-specific population mean of these tissues were estimated using the DARTEL (diffeomorphic anatomical registration through an exponentiated lie algebra) toolbox (Ashburner, 2007; Ashburner and Friston, 2009). For each subject, the contraction/expansion maps were multiplied with the probabilistic tissue segments, in within-subject average space, to generate percentage annual rate change maps. These were then warped using the above mentioned deformation composition to the MNI space and smoothed with a Gaussian kernel (8 mm full-width at half-maximum).

(VI) Correlation between functional and structural measurements in healthy controls and longitudinal change in nfvPPA. For each node of the intrinsic functional connectivity maps we extracted: (a) the *Z*-score for the connectivity to the epicentre from the group-level analysis in healthy controls; (b) the shortest intrinsic functional path to the epicentre; (c) the Euclidean distance from the epicentre; and (d) the average longitudinal grey matter change in nfvPPA patients.

We performed correlation analyses between the longitudinal grey matter volume change in nfvPPA and (a) the *Z*-score of the connectivity of each node with the epicentre; and (b) the shortest functional path from the epicentre in the healthy network. We used partial correlation to further control for the Euclidean distance between each node and the epicentre. The same analysis was performed for the default mode network. In this case, we used the seed region of interest defined in the precuneus as the epicentre. Finally, we repeated the same correlation analyses separately for the subset of nodes comprising each sub-network identified within the nfvPPA epicentre-anchored ICN. In these analyses, each node was referenced to the epicentre regardless of which subnetwork the node occupied.

For each subdivision of the white matter pathways reconstructed from the epicentre, we extracted: (a) the average fractional anisotropy value from the healthy fractional anisotropy map; and (b) the average of the relative longitudinal white matter change among the nfvPPAs.

The fractional anisotropy map was thresholded at 0.2 to restrict the analysis to white matter (Wakana *et al.*, 2005). We performed correlation analyses between these two measures in each tract. Our hypothesis was that as the spread followed structural connectivity patterns, higher fractional anisotropy values in the healthy brain would predict greater white matter longitudinal change in patients.

Results

Demographic and cognitive data

Demographic description and results of cognitive and language testing are reported in Table 1. Comparison between nfvPPA and control subjects revealed significant differences in several cognitive and linguistic scores consistent with the clinical profile of nfvPPA. These changes included significant impairments in speech fluency and the severity ratings of apraxia of speech and dysarthria ($P = 0.001$). Comparisons between performance at first presentation and at 1-year follow-up revealed significant worsening of speech and language performance consistent with clinical progression of nfvPPA. At 1-year follow-up (mean time interval ~384 days), patients showed significant changes in spontaneous speech fluency and severity ratings for apraxia of speech ($P = 0.001$) and sentence comprehension ($P = 0.05$). The early/mild nfvPPA group showed a similar, but milder pattern of worsening performance to the larger nfvPPA patient group.

Table 1 Demographic and cognitive evaluation

	NfvPPA ($n = 34$) Baseline	NfvPPA ($n = 34$) Follow-up	Controls ($n = 72$)
Age	68.6 (7.8)	69.6 (7.9)	64.8 (6.5)
Gender (F/M)	21/13	21/13	39/33
Handedness (R/L)	32/2	32/2	62/10
Education	16.1 (2.9)	16.1 (2.9)	17.5 (2.0)
Disease duration	3.57 (1.43)	4.6 (1.5)	N/A
MMSE (30)	25.0 (4.5)*	20.7 (7.8)†	29.6 (0.7)
CDR Total	0.48 (0.3)*	0.79 (0.7)†	N/A
Visuospatial function			
Benson copy (17)	14.6 (2.1)*	9.9 (3.4)†	15.8 (1.1)
Memory			
Benson Delay (17)	10.0(3.9)*	9.9 (4.5)†	12.2 (2.7)
CVLT-MS (10 min)	5.2 (2.8)*	4.4 (3.0)	7.6 (1.2)
CVLT-MS (recognition)	21.5 (7.0)*	17.9 (8.6)†	29.4 (4.5)
Executive function			
Digit Span Backwards	3.1 (1.4)*	2.5 (1.9)†	5.7 (1.4)
Modified Trails (lines /s)	0.2 (0.2)*	0.2 (0.2)†	0.6 (0.2)
Language			
Boston Naming Test (15)	11.5 (2.9)*	9.9 (4.2)†	14.5 (0.7)
Phonemic Fluency	4.9 (2.9)*	3.4 (2.4)†	17.4 (4.1)
Semantic Fluency	8.5 (4.8)*	6.9 (5.1)†	23.7 (5.6)
WAB Speech Fluency (10)	6.4 (2.5)*	4.9 (3.1)†	10 (0)
Repetition (WAB, 100)	81.5 (16.7)*	65.5 (31.3)†	100 (0)
AOS (MSE, 7 max)	2.6 (2.3)*	3.6 (2.2)†	0 (0)
Dysarthria (MSE, 7)	3.0 (2.7)*	2.9 (2.4)	0 (0)
PPTP (52)	49.1 (2.7)	47.3 (4.7)	51 (0.8)
Word Recognition (WAB, 60)	59.4 (0.9)	54.0 (12.9)†	60 (0)
Sequential Commands (80)	70.5 (10.3)*	61.7 (20.6)†	80 (0)
Syntax Comprehension (55)	46.5 (6.5)*	39.9 (10.5)†	54.8 (0.4)

*$P < 0.05$ patients versus controls; †$P < 0.05$ nvfPPA baseline versus follow-up.
AOS = apraxia of speech; CDR = clinical dementia rating; CVLT-MS = California Verbal Learning Test – Short Form; MMSE = Mini-Mental State Examination; MSE = Motor Speech Evaluation; PPTP = Pyramids and Palm Trees test Pictures; WAB = Western Aphasia Battery.

Image analyses

The left inferior frontal gyrus pars opercularis is the syndrome-specific epicentre in nfvPPA

VBM analysis in this early/mild group of nfvPPA compared to healthy controls showed the peak of early grey matter atrophy to be in the left inferior frontal gyrus and pars opercularis (IFGop, peak at $x = -48$, $y = 15$, $z = 23$; $Z = 7$) at $P < 0.05$, FWE corrected.

The functional network is anchored to the inferior frontal gyrus pars opercularis in the healthy brain

In healthy control subjects, the epicentre in IFGop was functionally connected, in the left hemisphere, with the inferior frontal gyrus triangularis and orbitalis, the middle frontal and the superior frontal gyri, the precentral cortex, and the paracentral lobule, including the supplementary motor area (SMA) and extending to the anterior midcingulate gyrus. The epicentre was also connected with the inferior parietal lobule, including the supramarginal gyrus, the middle/inferior temporal gyrus, anterior dorsal insula, and striatum. These left hemisphere areas are known to play a role in speech and language functions (Broca, 1865; Dronkers, 1996; Wilson *et al.*, 2010) and are typically damaged in nfvPPA (Grossman *et al.*, 1996; Nestor *et al.*, 2003; Gorno-Tempini *et al.*, 2006). The epicentre also had contralateral connections in the right inferior, middle and superior frontal gyri, the SMA, the supramarginal and angular gyri, the inferior temporal gyrus, and the caudate (Fig. 1A and Supplementary Table 1).

In healthy controls, the precuneus, a key node in the DMN, showed intrinsic connectivity to the medial orbital cortex, medial prefrontal cortex, posterior cingulate cortex, angular gyrus and the medial temporal lobe, as expected from previous studies (Greicius *et al.*, 2004; Damoiseaux *et al.*, 2006).

Structural connectivity of the inferior frontal gyrus pars opercularis in the healthy brain

In healthy controls, q-ball tractography delineated white matter pathways connecting the left IFGop with the inferior frontal gyrus triangular (IFGtr), the middle frontal gyrus, the superior frontal gyrus, the SMA, the inferior parietal gyrus and the temporal middle/inferior gyrus (Fig. 1B). Each subject's tractography was registered to MNI space. The main tracts involved were the aslant, the superior longitudinal fasciculus, and the arcuate fasciculus. These tracts are involved in speech and language functions and are damaged in nfvPPA (Galantucci *et al.*, 2011; Agosta *et al.*, 2013; Catani *et al.*, 2013; Grossman *et al.*, 2013; Mandelli *et al.*, 2014).

Graph theoretical network analysis of functional data in the healthy brain

The nodes of the graph were obtained by subdividing the intrinsic connectivity map into 8 mm^3 voxels, creating a total of 272 nodes. For each node, we extracted the correlation coefficient representing the strength of connectivity to the epicentre and calculated the shortest functional path length to the epicentre.

The modularity analysis showed three main subgraphs: Module 1 connects the inferior frontal gyri, the precentral gyrus and the SMA; Module 2 connects the inferior and superior parietal regions; and Module 3 connects the striatum and the SMA (Fig. 2A).

Structural connectivity underlying these subnetworks were represented by the bilateral aslant for Module 1, the left superior longitudinal fasciculus for Modules 1 and 2, the left arcuate fasciculus for Module 2, and tracts connecting the SMA and striatum and the IFGop and striatum for Module 3 (Fig. 2B).

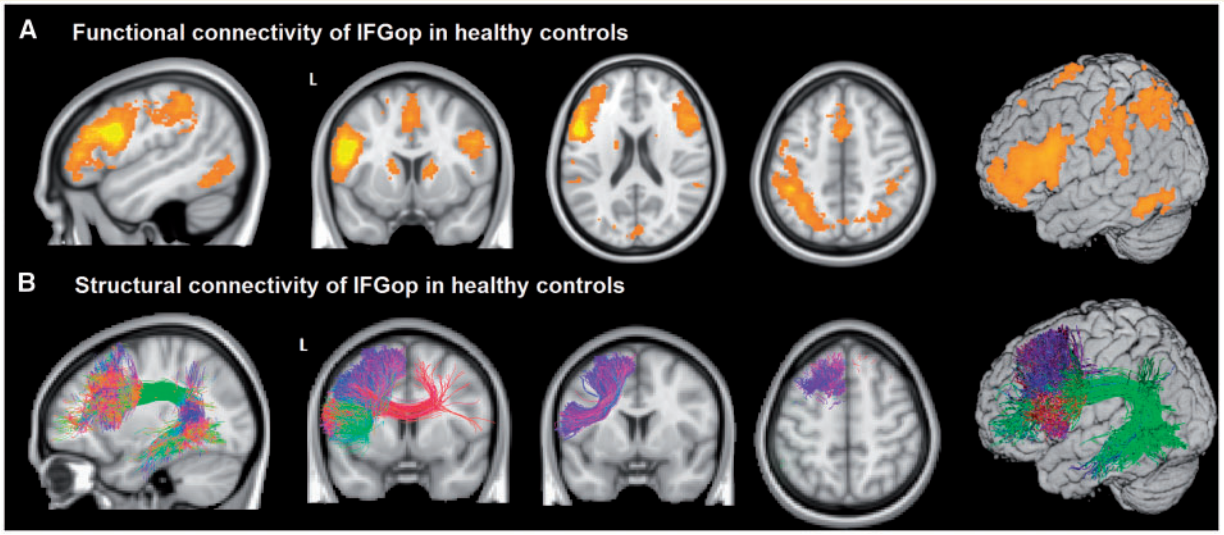

Figure 1 Functional and structural connectivity of IFGop in healthy controls. (**A**) An ICN map shows the functional connectivity of the IFGop with the supplementary motor cortex, basal ganglia and left inferior parietal areas and right inferior frontal gyrus. (**B**) Tractography shows the white matter pathways that structurally connect the IFGop with the IFGtr, the middle frontal gyrus, the superior frontal gyrus, the SMA, the inferior parietal gyrus and the temporal middle/inferior gyrus.

Longitudinal grey matter and white matter atrophy progression in nfvPPA

Significant longitudinal grey matter reduction was found in the left hemisphere in the precentral, inferior (pars opercularis and triangularis) middle and superior frontal gyri, SMA, inferior parietal regions (angular and supramarginal gyri), and in the striatum and thalamus. In the right hemisphere, changes were found in the inferior frontal gyrus (pars opercularis), precentral gyrus and SMA at $P < 0.05$, FWE corrected (Fig. 3A and Supplementary Table 2).

Significant longitudinal white matter reduction was shown mainly in the regions underlying the left frontal grey matter regions listed above, extending to the subcortical regions. Significance is reported at $P < 0.05$, FWE corrected (Fig. 3B). The white matter pathways corresponding to these areas were the tracts described above in the structural connectivity section.

Correlation between functional and structural measurements in healthy controls and longitudinal change in nfvPPA

Significant correlations were found between nodewise longitudinal grey matter volume reduction in patients and each node's strength of connectivity (*Z*-score) to the epicentre ($r = -0.3$, $P < 0.001$), or the path length to the syndrome-specific epicentre in the healthy controls ($r = 0.45$, $P < 0.001$; Fig. 4). This significance level remained after controlling for Euclidean distance from the epicentre. No significant correlation was found in the DMN with the *Z*-score ($r = 0.003$, $P = 0.9$) nor with path length ($r = -0.12$, $P = 0.2$; Fig. 4).

Within the three modules identified in the ICN anchored by the IFGop, significant correlation between longitudinal grey matter atrophy and the strength of the functional connectivity in controls was found only in Module 1 ($r = -0.3$, $P = 0.001$; Fig. 5). However, the path length correlations with longitudinal change were significant in all three modules. In Module 1 ($r = 0.52$, $P < 0.001$) and Module 3 ($r = 0.53$, $P < 0.001$) the significance survived Euclidean distance correction, while in Module 2 ($r = 0.37$, $P < 0.001$), it did not survive after Euclidean correction.

Significant correlations were found between longitudinal white matter change and the healthy fractional anisotropy within the following structural pathways defined in the group of healthy subjects: in the left aslant tract ($r = -0.73$, $P < 0.001$) and in the left superior longitudinal fasciculus ($r = -0.6$, $P < 0.001$), but not in the left arcuate fasciculus ($r = -0.03$, $P = 0.57$). In Fig. 6 we show the scatterplot of the correlations within these tracts.

Discussion

In the present multimodal neuroimaging study, we showed that atrophy progression in nfvPPA occurs within specific functional and structural large-scale network that sustain speech production. Our analyses demonstrated that the brain regions that showed the most significant longitudinal grey matter atrophy in nfvPPA were also the ones most strongly functionally and structurally connected to the syndrome-specific epicentre in the healthy brain. Specifically, starting from the left IFGop, atrophy progressed most

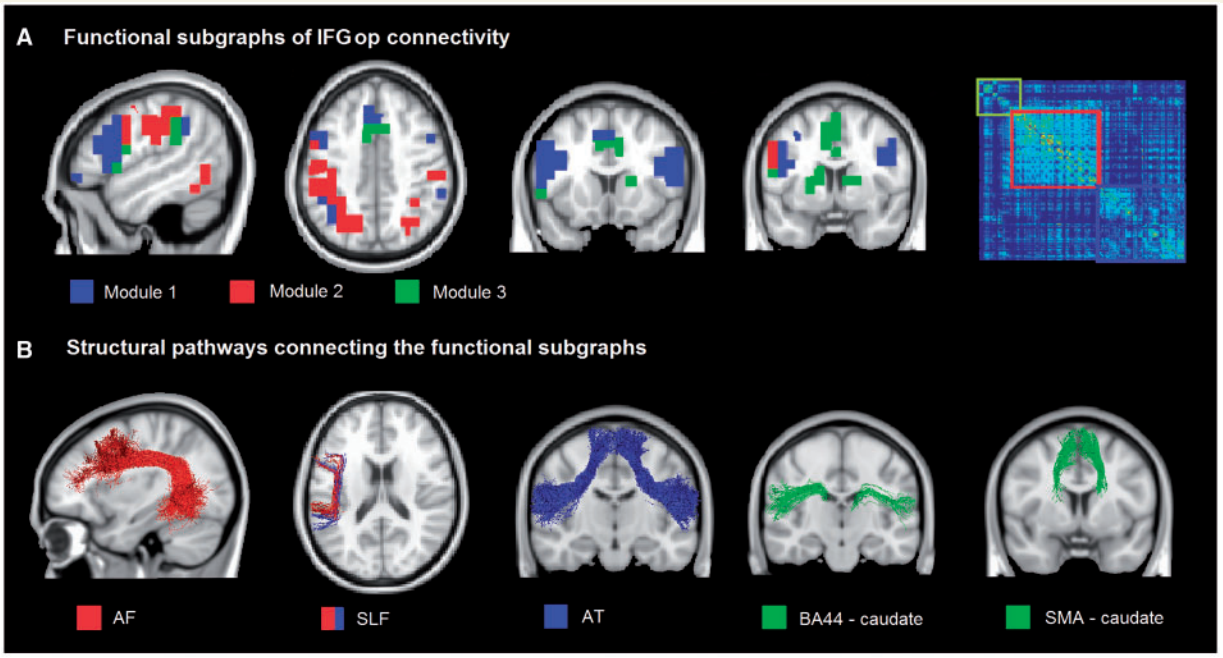

Figure 2 Functional and structural subdivision of the network connecting the IFGop. (**A**) Three functional subgraphs were identified: Module 1 (blue) connects bilaterally the inferior frontal gyrus and the SMA; Module 2 (red) connects bilaterally the inferior and superior parietal regions; and Module 3 (green) connects bilaterally the striatum and the SMA. On the right, the connection matrix is presented with the nodes reordered according to an optimal modularity partition (Louvain method). (**B**) Specific tracts underlying these sub-graphs are the bilateral aslant tract (AT), the left superior longitudinal fasciculus (SLF), the left arcuate fasciculus (AF), the bilateral tracts connecting the SMA with the striatum, and the inferior frontal gyrus pars opercularis with the striatum.

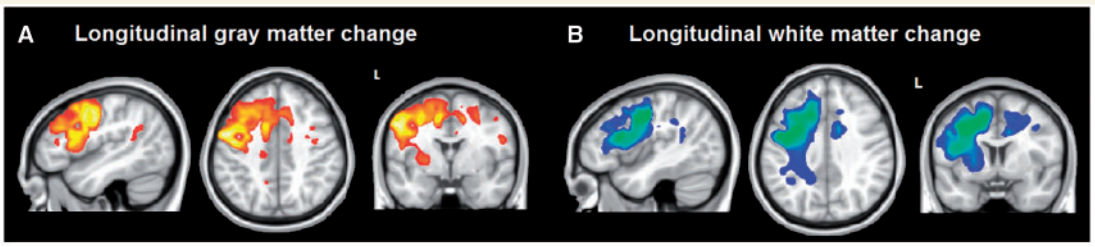

Figure 3 Statistical parametric map (T-statistic) of longitudinal changes in grey and white matter volume in nfvPPA compared to controls. (**A**) Longitudinal grey matter changes were found to be significant in the left premotor cortex, the left IFGop, the left middle frontal gyrus, the left SMA, the left angular gyrus, the right inferior frontal gyrus (p. opercularis and p. triangularis), the left thalamus, the right cingulate, and in the right premotor cortex at $P < 0.05$, FWE corrected. (**B**) Longitudinal white matter changes in the subcortical white matter regions extending under the grey matter regions were found to be significant at $P < 0.05$, FWE corrected.

significantly to the SMA through the aslant tract. Taken together, our results strongly suggest that neurodegeneration starts in a syndrome-specific epicentre and then spreads to the most connected regions following neuronal network architecture.

We discuss these findings in the context of previous evidence regarding the speech and language systems in the brain and the transneuronal spread model.

The syndrome-specific epicentre in nfvPPA

We identified the syndrome-specific epicentre in nfvPPA as a small dorsal portion of the opercular region of the left inferior frontal gyrus. This region was selectively atrophied in a group of patients with the mildest disease (with Clinical Dementia Rating of 0), demonstrating greater susceptibility of this region to the disorder. This epicentre is included in the area of atrophy shown in several previous nfvPPA studies (Gorno-Tempini *et al.*, 2004, 2006; Grossman, 2012). In a previous study, Zhou *et al.* (2012) sought regions, referred to as epicentres, whose functional connectivity in healthy controls most closely mirrored the pattern of atrophy in nfvPPA; these analyses also identified the IFGop, among other regions, as a key epicentre in nfvPPA. Why the IFGop is most vulnerable to disease is still not known. The pars opercularis is the most posterior part of the inferior frontal gyrus, a region recognized

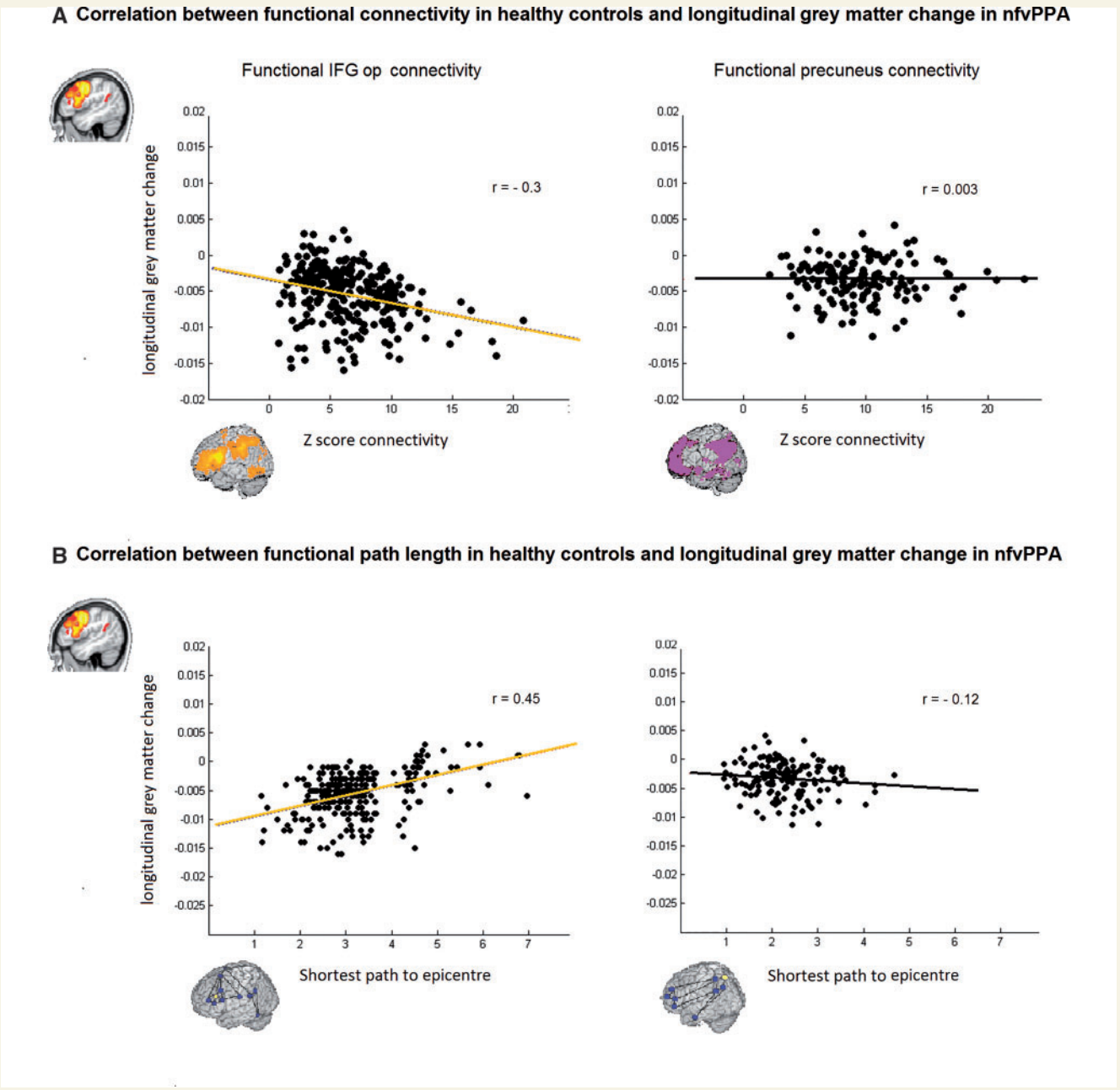

Figure 4 Scatter plots of the correlations between functional connectivity strength and shortest functional path length from the epicentre in healthy controls and grey matter longitudinal change in nfvPPA. (**A**) Significant correlation with direct functional connectivity (*Z*-score) was found in the functional IFGop connectivity ($r = -0.3$, $P < 0.001$) but not in the functional precuneus connectivity ($r = 0.003$, $P = 0.9$). (**B**) Significant correlation with the shortest path length was found in the functional IFGop connectivity ($r = -0.45$, $P < 0.001$) but not in the functional precuneus connectivity ($r = -0.12$, $P = 0.2$).

as important for speech production since Broca's first functional-anatomical observations in 1861 (Broca, 1861). More than a century of neuropsychological and functional imaging studies have refined the role of this region, which is essential for articulation and motor speech execution (Davis *et al.*, 2008; Flinker *et al.*, 2015). Cytoarchitectonically, the IFGop corresponds to Brodmann's area 44 (BA44), which is dysgranular cortex, reflecting a paucity of small pyramidal neurons in layer IV. BA44 is also defined as a 'transition cortex' between agranular ventral premotor regions (BA6) and granular dorsal (BA9) and ventral (BA45 or IFGtr) association cortices (Mesulam and Mufson, 1982; Amunts *et al.*, 1999). It has been hypothesized that this type of transitional cortex is particularly susceptible to FTLD-type pathology, as seen in the transitional anterior insular and cingulate cortices that represent the critical epicentres in behavioural variant FTD (bvFTD) (Seeley, 2008; Zhou *et al.*, 2012). Recent clinico-pathological studies indicate that nfvPPA is most often caused by FTLD-tau-type pathology (Josephs *et al.*,

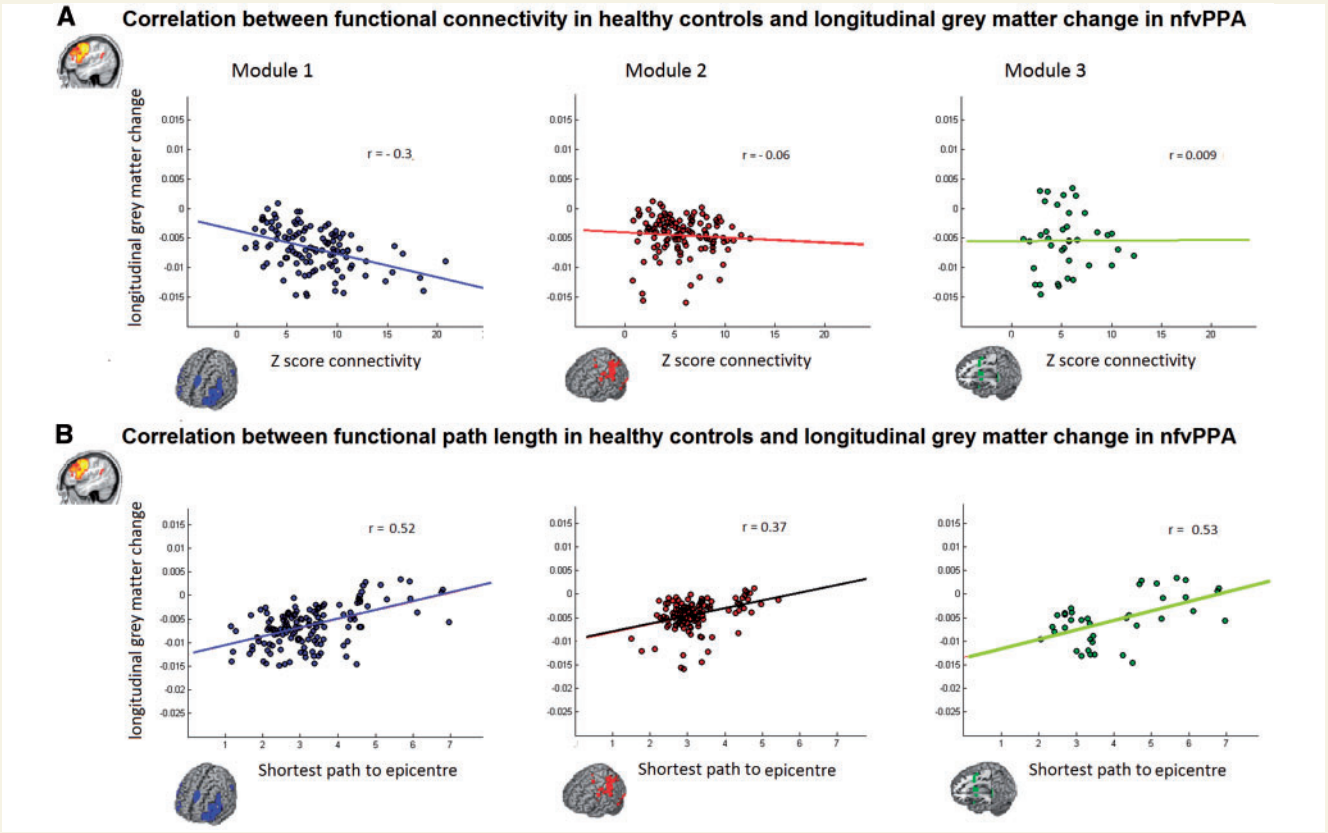

Figure 5 Scatter plots of the correlations between functional connectivity strength and shortest functional path length to the epicentre in healthy controls and grey matter longitudinal change in nfvPPA in the three different modules. (**A**) Significant correlation with direct functional connectivity (*Z*-score) was found only in Module 1 ($r = -0.3$, $P < 0.001$). (**B**) Significant correlations with the shortest path length were found in all the three different modules (Module 1, $r = 0.52$, $P < 0.001$; Module 2, $r = 0.37$, $P < 0.001$ and Module 3, $r = 0.53$, $P < 0.001$).

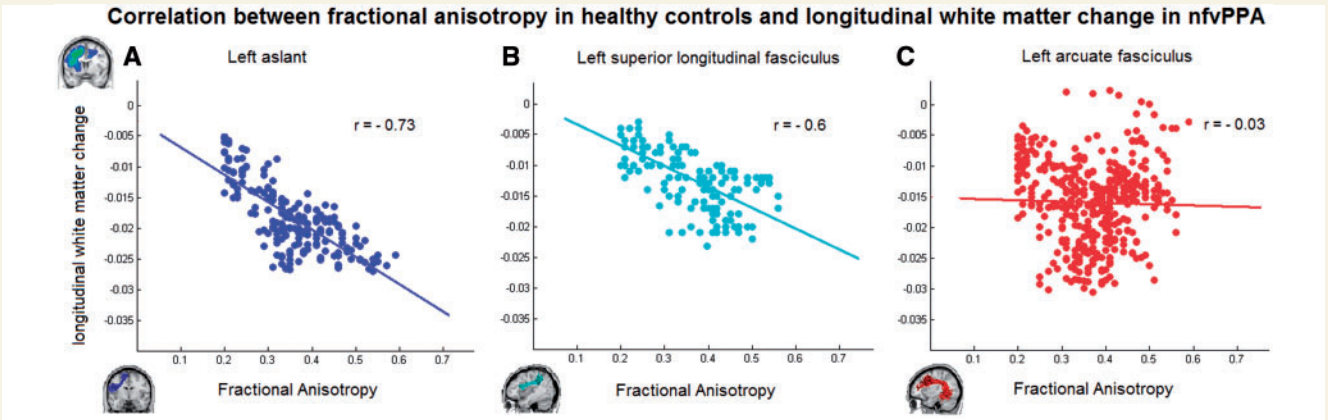

Figure 6 Scatter plots of the correlations between fractional anisotropy in healthy controls along the structural pathways and white matter longitudinal change in nfvPPA. (**A**) Left aslant tract ($r = -0.73$ $P < 0.001$). (**B**) Left superior longitudinal fasciculus ($r = -0.6$, $P < 0.001$). (**C**) Left arcuate fasciculus ($r = -0.03$, $P = 0.57$).

2006; Mesulam *et al.*, 2008; Grossman, 2011; Caso *et al.*, 2014; Santos-Santos *et al.*, 2016). In our sample, 21 of 23 cases with pathological confirmation had FTLD-tau and none had evidence of Alzheimer's disease as a primary cause of pathology or *in vivo* biomarkers. Whether there is a specific IFGop cell population susceptible to FTLD remains unknown. Further studies elucidating the vulnerability of this epicentre region to FTLD degeneration, and in particular FTLD-tau might provide important clues to the pathogenesis of disease. As tau is the most common

cause of nfvPPA and is consistently shown to spread transsynaptically in laboratory studies, nfvPPA might provide an appropriate model to study the transneuronal spread *in vivo*.

Structural and functional networks anchored to the nfvPPA epicentre in healthy controls

Tractography and intrinsic functional connectivity network analyses allowed us to identify the networks anchored by the IFGop epicentre in healthy controls. Q-ball tractography results highlighted a system of short and longwhite matter pathways connecting intra-frontal, insular, basal ganglia and parietal regions. These findings are consistent with previous animal and human studies (Catani *et al.*, 2012; Thiebaut de Schotten *et al.*, 2012). In particular, the epicentre in the left IFGop was connected with the SMA through the aslant tract, the inferior parietal lobule through the superior longitudinal fasciculus, and the posterior temporal region through the arcuate fasciculus. Previous diffusion tensor imaging (DTI) tractography studies have shown the involvement of these three left hemisphere white matter pathways in specific language functions (Hickok and Poeppel, 2007; Patterson *et al.*, 2007; Wilson *et al.*, 2011). Consistent with the fact that these tracts were dissected starting from the nfvPPA epicentre, previous DTI studies in nfvPPA have shown that these tracts are the ones typically damaged in this PPA variant (Whitwell *et al.*, 2010; Galantucci *et al.*, 2011; Grossman, 2012; Mahoney *et al.*, 2013; Sajjadi *et al.*, 2013; Schwindt *et al.*, 2013). In addition, the IFGop connected to its homologous region in the contralateral hemisphere through the corpus callosum. Fractional anisotropy values from each of these tracts were extracted as indexes of the strength of structural connectivity along the pathways connecting the IFGop epicentre with more distant regions.

Seed-based, intrinsic connectivity analysis of functional neuroimaging data at rest showed a large-scale coherence pattern between the anatomically connected cortical and striatal regions (Fig. 1A and B). Coherence within this network of predominantly left-hemisphere regions is crucial for many speech and language functions (Binder *et al.*, 1997; Vigneau *et al.*, 2006; Price, 2010). However, previous studies on the neural basis of language, and the selective atrophy pattern typical of nfvPPA, suggest that within this overall fronto-striatal-temporo-parietal network, there would likely be anatomical and functional subnetworks specialized for different speech and language functions (Binder *et al.*, 1997; Friederici, 2011). To identify these subnetworks within the overall seed-derived connectivity pattern, we applied graph theoretical approaches. We identified three modules (or subgraphs) comprising the IFGop and the SMA/prefrontal regions, IFGop and the inferior parietal area and the SMA and striatal regions (Fig. 2). Indices of connectivity strength to the epicentre (correlations with the epicentre from the seed-based analyses and path length from the graphs) were extracted from each node, then examined collectively and on a per-module basis.

The relationship between longitudinal atrophy in nfvPPA and structural and functional connectivity in healthy controls

The main goal of our study was to relate functional and structural connectivity strengths between the epicentre and its connected regions in the healthy brain to the pattern of longitudinal grey and white matter atrophy in nfvPPA. Previous studies have used cross-sectional neuroimaging data to predict gradients of atrophy with either functional (ICN-MRI; Zhou *et al.*, 2012) or structural (diffusion-weighted imaging; Raj *et al.*, 2012) connectivity in healthy subjects. To our knowledge, the present study is the first to relate both functional and structural network connectivity with longitudinal atrophy changes. This approach could provide more direct evidence in favour of within-network connectivity-based disease spread. In particular, the transneuronal spread hypothesis predicts that longitudinal atrophy changes would be greater in grey and white matter structures with greater connectivity strength to the nfvPPA syndrome-specific epicentre. Based on the results of the network analyses in healthy subjects, we predicted that the most severe longitudinal changes would occur in regions included in the subgraph connecting the IFGop to the SMA/prefrontal (Fig. 2).

Results of the longitudinal atrophy changes in nfvPPA showed that, 1 year after the first visit, there was significant atrophy progression in large areas. Particularly affected were grey and white matter in the left posterior frontal regions (comprising inferior middle and superior gyri), SMA, insula, striatum, inferior parietal regions and underlying white matter. These results are consistent with the few previous longitudinal neuroimaging studies in PPA (Rogalski *et al.*, 2011; Brambati *et al.*, 2015; Santos-Santos *et al.*, 2016) and largely overlap anatomically with the structural and functional networks described in healthy adults (Figs 1 and 2). To explore more directly the relationship between strength of connectivity in healthy subjects and degree of longitudinal change in patients, we correlated indices of connectivity and atrophy progression in corresponding nodes and pathways. In particular, functional connectivity strength values and fractional anisotropy within the white matter tracts of interest from the healthy network were correlated with longitudinal grey and white matter changes, respectively. First, we showed that overall functional connectivity indices within the network anchored to the left IFGop (correlation with the epicentre from the seed-based analyses and path length from the graphs) correlated to longitudinal MRI changes in nfvPPA, while connectivity within a control network (the

default network) did not. This finding suggests that trans-neuronal spread of disease occurs selectively within the network anchored to the syndrome epicentre. Furthermore, we showed that the strongest correlation between structural and functional connectivity and longitudinal change occured in the first module connecting the IFGop to the SMA and prefrontal regions through the aslant (Fig. 5). This pathway presented the most significant white matter longitudinal change in nfvPPA compared to the other language pathways and the most significant correlation with the index of structural integrity. The aslant tract plays a role in the initiation and execution of movements, especially articulation and, in nfvPPA, its integrity correlated with the amount of distortion errors that patients made in spontaneous speech (Mandelli *et al.*, 2014). The SMA is also part of a frontostriatal network involved in general motor control, sequencing and response selection processes (Chung *et al.*, 2005; Alario *et al.*, 2006; Kim *et al.*, 2010). It is noteworthy that the direct functional connectivity with the epicentre (*Z*-score) within the dorsal fronto-parietal and the fronto-striatal subgraphs did not correlate significantly with longitudinal grey matter changes, while all of them showed a significant correlation with the shortest functional path to the network epicentre. These results suggest that progression is most accurately predicted by a model of spread as propagation along multi-step paths from the epicentre rather than by direct connections to the epicentre. Nodes within the epicentre-containing IFG/SMA subnetwork are most likely to have their shortest paths to the epicentre be direct connections, hence the significant correlation of direct functional connectivity and longitudinal volume changes only in that module. Nodes in the striatal and dorsal frontoparietal subnetworks instead have a weaker relationship between direct functional connectivity and longitudinal volume changes but still show significant correlation with the path length, as it becomes more likely that a multi-step path is taken from the epicentre, rather than a relatively weak direct connection. In these modules, the path length-based model of spread outperformed the direct functional connectivity model. Taken together, all these findings suggest that, at least in the early stages, the disease progresses most significantly to frontal grey matter areas devoted to motor control and executive functioning, and later in the disease extends into networks with stronger functional relationships to the primary one. Consistently, the nfvPPA clinical syndrome most often progresses to more severe motor speech and grammatical deficits and to more general motor and executive dysfunction, such as corticobasal syndrome or progressive supranuclear syndrome (Kertesz, 2006; Lee *et al.*, 2011). Although the superior longitudinal fasciculus and SMA-striatal connections also showed significant correlations, the strongest result occurred in the aslant, which was also the tract with the greatest longitudinal white matter change. One might speculate that toxic disease proteins spread from the grey matter epicentre into axons of white matter pathways through the aslant to the SMA, the next most connected grey matter node.

This study presents some limitations. First, resting-state functional MRI and DTI-derived metrics are indirect *in vivo* indexes of connectivity strength. In particular, structural connectivity measures have been less widely applied and there is no consensus on which DTI-derived metrics should be used. We chose fractional anisotropy because previous evidence suggests that it is the most reliable of the DTI-derived metrics, while axial and radial diffusivity might introduce a systematic bias leading to incorrect estimation (Pierpaoli and Basser, 1996; Wheeler-Kingshott and Cercignani, 2009). The alternative of using number of streamlines per tract is, in our view, even more problematic as it is prone to variability due to acquisition and tracking techniques. Finally, longitudinal atrophy changes are only proxies for neuronal loss caused by the spread of toxic proteins. *In vivo* molecular imaging techniques, such as tau PET, will likely be able to directly track the spread of disease protein aggregates in the human brain.

In conclusion, we showed that longitudinal atrophy changes in nfvPPA follow the architecture of the speech production functional and structural large-scale network in the healthy brain. These findings support the hypothesis that neurodegeneration progresses through trans-synaptic spread in predetermined, connected neuronal networks.

Acknowledgements

The authors thank the patients and their families for the time and effort they dedicated to the research.

Funding

The study was supported by grants from the National Institutes of Health (NINDS R01 NS050915, NIA P50 AG03006, NIA P50 AG023501, NIA P01 AG019724); State of California (DHS04-35516); Alzheimer's Disease Research Centre of California (03–75271 DHS/ADP/ARCC); Larry L. Hillblom Foundation; John Douglas French Alzheimer's Foundation; Koret Family Foundation; Consortium for Frontotemporal Dementia Research; and McBean Family Foundation and a Career Scientist Award (NFD) from the US Department of Veterans Affairs Clinical Sciences R&D Program. These supporting sources had no involvement in the study design, collection, analysis or interpretation of data, nor were they involved in writing the paper or the decision to submit this report for publication.

Supplementary material

Supplementary material is available at *Brain* online.

References

Agosta F, Galantucci S, Canu E, Cappa SF, Magnani G, Franceschi M, et al. Disruption of structural connectivity along the dorsal and ventral language pathways in patients with nonfluent and semantic variant primary progressive aphasia: a DT MRI study and a literature review. Brain Lang 2013; 127: 157–66.

Alario FX, Chainay H, Lehericy S, Cohen L. The role of the supplementary motor area (SMA) in word production. Brain Res 2006; 1076: 129–43.

Amunts K, Schleicher A, Burgel U, Mohlberg H, Uylings HB, Zilles K. Broca's region revisited: cytoarchitecture and intersubject variability. J Comp Neurol 1999; 412: 319–41.

Ashburner J. A fast diffeomorphic image registration algorithm. Neuroimage 2007; 38: 95–113.

Ashburner J, Friston KJ. Computing average shaped tissue probability templates. Neuroimage 2009; 45: 333–41.

Ashburner J, Ridgway GR. Symmetric diffeomorphic modeling of longitudinal structural MRI. Front Neurosci 2012; 6: 197.

Berman JI, Chung S, Mukherjee P, Hess CP, Han ET, Henry RG. Probabilistic streamline q-ball tractography using the residual bootstrap. Neuroimage 2008; 39: 215–22.

Binder JR, Frost JA, Hammeke TA, Cox RW, Rao SM, Prieto T. Human brain language areas identified by functional magnetic resonance imaging. J Neurosci 1997; 17: 353–62.

Blondel VD, Guillaume JL, Hendrickx JM, de Kerchove C, Lambiotte R. Local leaders in random networks. Phys Rev E Stat Nonlin Soft Matter Phys 2008; 77(3 Pt 2): 036114.

Brambati SM, Amici S, Racine CA, Neuhaus J, Miller Z, Ogar J, et al. Longitudinal gray matter contraction in three variants of primary progressive aphasia: a tenser-based morphometry study. Neuroimage Clin 2015; 8: 345–55.

Broca P. Remarques sur le siege de la faculte du langage articule, suivies d'une observation d'aphemie. Bull Soc Anatomique 1861; 2: 330–57.

Broca P. Sur la faculte du langage articule. Bull Soc Anthrop Paris 1865; 6: 337–93.

Caso F, Mandelli ML, Henry M, Gesierich B, Bettcher BM, Ogar J, et al. In vivo signatures of nonfluent/agrammatic primary progressive aphasia caused by FTLD pathology. Neurology 2014; 82: 239–47.

Catani M, Dell'acqua F, Vergani F, Malik F, Hodge H, Roy P, et al. Short frontal lobe connections of the human brain. Cortex 2012; 48: 273–91.

Catani M, Mesulam MM, Jakobsen E, Malik F, Martersteck A, Wieneke C, et al. A novel frontal pathway underlies verbal fluency in primary progressive aphasia. Brain 2013; 136 (Pt 8): 2619–28.

Chung GH, Han YM, Jeong SH, Jack CR Jr. Functional heterogeneity of the supplementary motor area. Am J Neuroradiol 2005; 26: 1819–23.

Clavaguera F, Bolmont T, Crowther RA, Abramowski D, Frank S, Probst A, et al. Transmission and spreading of tauopathy in transgenic mouse brain. Nat Cell Biol 2009; 11: 909–13.

Curtiss S, Yamada J. Curtiss-Yamada Comprehensive Language Evaluation. Unpublished test; 1988. Retrieved May 22, 2007, from http://thecycletest.com.

Damoiseaux JS, Rombouts SA, Barkhof F, Scheltens P, Stam CJ, Smith SM, et al. Consistent resting-state networks across healthy subjects. Proc Natl Acad Sci USA 2006; 103: 13848–53.

Davis C, Kleinman JT, Newhart M, Gingis L, Pawlak M, Hillis AE. Speech and language functions that require a functioning Broca's area. Brain Lang 2008; 105: 50–8.

de Calignon A, Polydoro M, Suarez-Calvet M, William C, Adamowicz DH, Kopeikina KJ, et al. Propagation of tau pathology in a model of early Alzheimer's disease. Neuron 2012; 73: 685–97.

Dronkers NF. A new brain region for coordinating speech articulation. Nature 1996; 384: 159–61.

Flinker A, Korzeniewska A, Shestyuk AY, Franaszczuk PJ, Dronkers NF, Knight RT, et al. Redefining the role of Broca's area in speech. Proc Natl Acad Sci USA 2015; 112: 2871–5.

Friederici AD. The brain basis of language processing: from structure to function. Physiol Rev 2011; 91: 1357–92.

Frost B, Diamond MI. Prion-like mechanisms in neurodegenerative diseases. Nat Rev Neurosci 2010; 11: 155–9.

Galantucci S, Tartaglia MC, Wilson SM, Henry ML, Filippi M, Agosta F, et al. White matter damage in primary progressive aphasias: a diffusion tensor tractography study. Brain 2011; 134 (Pt 10): 3011–29.

Gorno-Tempini ML, Dronkers NF, Rankin KP, Ogar JM, Phengrasamy L, Rosen HJ, et al. Cognition and anatomy in three variants of primary progressive aphasia. Ann Neurol 2004; 55: 335–46.

Gorno-Tempini ML, Hillis AE, Weintraub S, Kertesz A, Mendez M, Cappa SF, et al. Classification of primary progressive aphasia and its variants. Neurology 2011; 76: 1006–14.

Gorno-Tempini ML, Ogar JM, Brambati SM, Wang P, Jeong JH, Rankin KP, et al. Anatomical correlates of early mutism in progressive nonfluent aphasia. Neurology 2006; 67: 1849–51.

Greicius MD, Srivastava G, Reiss AL, Menon V. Default-mode network activity distinguishes Alzheimer's disease from healthy aging: evidence from functional MRI. Proc Natl Acad Sci USA 2004; 101: 4637–42.

Grossman M. Biomarkers to identify the pathological basis for frontotemporal lobar degeneration. J Mol Neurosci 2011; 45: 366–71.

Grossman M. The non-fluent/agrammatic variant of primary progressive aphasia. Lancet Neurol 2012; 11: 545–55.

Grossman M, Mickanin J, Onishi K, Hughes E, D'Esposito M, Ding XS, et al. Progressive nonfluent aphasia: language, cognitive, and pet measures contrasted with probable Alzheimer's disease. J Cogn Neurosci 1996; 8: 135–54.

Grossman M, Powers J, Ash S, McMillan C, Burkholder L, Irwin D, et al. Disruption of large-scale neural networks in non-fluent/agrammatic variant primary progressive aphasia associated with frontotemporal degeneration pathology. Brain Lang 2013; 127: 106–20.

Hallquist MN, Hwang K, Luna B. The nuisance of nuisance regression: spectral misspecification in a common approach to resting-state fMRI preprocessing reintroduces noise and obscures functional connectivity. Neuroimage 2013; 82: 208–25.

Hickok G, Poeppel D. The cortical organization of speech processing. Nat Rev Neurosci 2007; 8: 393–402.

Josephs KA, Duffy JR, Strand EA, Whitwell JL, Layton KF, Parisi JE, et al. Clinicopathological and imaging correlates of progressive aphasia and apraxia of speech. Brain 2006; 129 (Pt 6): 1385–98.

Kertesz A. Western aphasia battery. London, Ontario: University of Western Ontario Press; 1980.

Kertesz A. Progress in clinical neurosciences: Frontotemporal dementia-pick's disease. Can J Neurol Sci 2006; 33: 141–8.

Kim JH, Lee JM, Jo HJ, Kim SH, Lee JH, Kim ST, et al. Defining functional SMA and pre-SMA subregions in human MFC using resting state fMRI: functional connectivity-based parcellation method. Neuroimage 2010; 49: 2375–86.

Kramer JH, Jurik J, Sha SJ, Rankin KP, Rosen HJ, Johnson JK, et al. Distinctive neuropsychological patterns in frontotemporal dementia, semantic dementia, and Alzheimer disease. Cogn Behav Neurol 2003; 16: 211–18.

Lee SE, Rabinovici GD, Mayo MC, Wilson SM, Seeley WW, Dearmond SJ, et al. Clinicopathological correlations in corticobasal degeneration. Ann Neurol 2011; 70: 327–40.

Liu L, Drouet V, Wu JW, Witter MP, Small SA, Clelland C, et al. Trans-synaptic spread of tau pathology in vivo. PLoS One 2012; 7: e31302.

Mack WJ, Freed DM, Williams BW, Henderson VW. Boston naming test: shortened versions for use in Alzheimer's disease. J Gerontol 1992; 47: P154–8.

Mahoney CJ, Malone IB, Ridgway GR, Buckley AH, Downey LE, Golden HL, et al. White matter tract signatures of the progressive aphasias. Neurobiol Aging 2013; 34: 1687–99.

Mandelli ML, Caverzasi E, Binney RJ, Henry ML, Lobach I, Block N, et al. Frontal white matter tracts sustaining speech production in primary progressive aphasia. J Neurosci 2014; 34: 9754–67.

Mandelli ML, Vitali P, Santos M, Henry M, Gola K, Rosenberg L, et al. Two insular regions are differentially involved in behavioral variant FTD and nonfluent/agrammatic variant PPA. Cortex 2016; 74: 149–57.

Mesulam M, Wicklund A, Johnson N, Rogalski E, Leger GC, Rademaker A, et al. Alzheimer and frontotemporal pathology in subsets of primary progressive aphasia. Ann Neurol 2008; 63: 709–19.

Mesulam MM, Mufson EJ. Insula of the old world monkey. I. Architectonics in the insulo-orbito-temporal component of the paralimbic brain. J Comp Neurol 1982; 212: 1–22.

Nestor PJ, Graham NL, Fryer TD, Williams GB, Patterson K, Hodges JR. Progressive non-fluent aphasia is associated with hypometabolism centred on the left anterior insula. Brain 2003; 126 (Pt 11): 2406–18.

Newman ME. Modularity and community structure in networks. Proc Natl Acad Sci USA 2006; 103: 8577–82.

Patterson K, Nestor PJ, Rogers TT. Where do you know what you know? The representation of semantic knowledge in the human brain. Nat Rev Neurosci 2007; 8: 976–87.

Pierpaoli C, Basser PJ. Toward a quantitative assessment of diffusion anisotropy. Magn Reson Med 1996; 36: 893–906.

Price CJ. The anatomy of language: a review of 100 fMRI studies published in 2009. Ann NY Acad Sci 2010; 1191: 62–88.

Raj A, Kuceyeski A, Weiner M. A network diffusion model of disease progression in dementia. Neuron 2012; 73: 1204–15.

Rogalski E, Cobia D, Harrison TM, Wieneke C, Weintraub S, Mesulam MM. Progression of language decline and cortical atrophy in subtypes of primary progressive aphasia. Neurology 2011; 76: 1804–10.

Rosen HJ, Gorno-Tempini ML, Goldman WP, Perry RJ, Schuff N, Weiner M, et al. Patterns of brain atrophy in frontotemporal dementia and semantic dementia. Neurology 2002; 58: 198–208.

Rubinov M, Sporns O. Complex network measures of brain connectivity: uses and interpretations. Neuroimage 2010; 52: 1059–69.

Sajjadi SA, Acosta-Cabronero J, Patterson K, Diaz-de-Grenu LZ, Williams GB, Nestor PJ. Diffusion tensor magnetic resonance imaging for single subject diagnosis in neurodegenerative diseases. Brain 2013; 136 (Pt 7): 2253–61.

Santos-Santos MA, Mandelli M, Binney RJ, Ogar J, Henry M, Hubbard HI, et al. Cross-sectional and longitudinal features of non-fluent/agrammatic primary progressive aphasia with underlying corticobasal degeneration or progressive supranuclear palsy pathology. JAMA Neurol 2016; 73: 733–42.

Satterthwaite TD, Elliott MA, Gerraty RT, Ruparel K, Loughead J, Calkins ME, et al. An improved framework for confound regression and filtering for control of motion artifact in the preprocessing of resting-state functional connectivity data. Neuroimage 2013; 64: 240–56.

Schwindt GC, Graham NL, Rochon E, Tang-Wai DF, Lobaugh NJ, Chow TW, et al. Whole-brain white matter disruption in semantic and nonfluent variants of primary progressive aphasia. Hum Brain Map 2013; 34: 973–84.

Seeley WW. Selective functional, regional, and neuronal vulnerability in frontotemporal dementia. Curr Opin Neurol 2008; 21: 701–7.

Seeley WW, Crawford RK, Zhou J, Miller BL, Greicius MD. Neurodegenerative diseases target large-scale human brain networks. Neuron 2009; 62: 42–52.

Thiebaut de Schotten M, Dell'Acqua F, Valabregue R, Catani M. Monkey to human comparative anatomy of the frontal lobe association tracts. Cortex 2012; 48: 82–96.

Thomas AG, Marrett S, Saad ZS, Ruff DA, Martin A, Bandettini PA. Functional but not structural changes associated with learning: an exploration of longitudinal voxel-based morphometry (VBM). Neuroimage 2009; 48: 117–25.

Vigneau M, Beaucousin V, Herve PY, Duffau H, Crivello F, Houde O, et al. Meta-analyzing left hemisphere language areas: phonology, semantics, and sentence processing. Neuroimage 2006; 30: 1414–32.

Wakana S, Nagae-Poetscher LM, Jiang H, van Zijl P, Golay X, Mori S. Macroscopic orientation component analysis of brain white matter and thalamus based on diffusion tensor imaging. Magn Reson Med 2005; 53: 649–57.

Wheeler-Kingshott CA, Cercignani M. About "axial" and "radial" diffusivities. Magn Reson Med 2009; 61: 1255–60.

Whitwell JL, Avula R, Senjem ML, Kantarci K, Weigand SD, Samikoglu A, et al. Gray and white matter water diffusion in the syndromic variants of frontotemporal dementia. Neurology 2010; 74: 1279–87.

Wilson SM, Galantucci S, Tartaglia MC, Rising K, Patterson DK, Henry ML, et al. Syntactic processing depends on dorsal language tracts. Neuron 2011; 72: 397–403.

Wilson SM, Henry ML, Besbris M, Ogar JM, Dronkers NF, Jarrold W, et al. Connected speech production in three variants of primary progressive aphasia. Brain 2010; 133 (Pt 7): 2069–88.

Yushkevich PA, Avants BB, Das SR, Pluta J, Altinay M, Craige C. Bias in estimation of hippocampal atrophy using deformation-based morphometry arises from asymmetric global normalization: an illustration in ADNI 3 T MRI data. Neuroimage 2010; 50: 434–45.

Zhou J, Gennatas ED, Kramer JH, Miller BL, Seeley WW. Predicting regional neurodegeneration from the healthy brain functional connectome. Neuron 2012; 73: 1216–27.